Materials Characterization 117 (2016) 113–126

Contents lists available at ScienceDirect

Materials Characterization

journal homepage: www.elsevier.com/locate/matchar

Tutorial: Crystal orientations and EBSD — Or which way is up?

T.B. Britton [a,*], J. Jiang [a], Y. Guo [b,1], A. Vilalta-Clemente [b], D. Wallis [c], L.N. Hansen [c], A. Winkelmann [d], A.J. Wilkinson [b]

[a] Department of Materials, Imperial College London, Prince Consort Road, SW7 2AZ, United Kingdom
[b] Department of Materials, University of Oxford, Parks Road, OX1 3PH, United Kingdom
[c] Department of Earth Sciences, University of Oxford, South Parks Road, OX1 3AN, United Kingdom
[d] Bruker Nano GmbH, Am Studio 2D, 12489 Berlin, Germany

ARTICLE INFO

Article history:
Received 19 November 2015
Received in revised form 28 February 2016
Accepted 15 April 2016
Available online 20 April 2016

Keywords:
Electron backscatter diffraction
Crystal orientation
Texture
Electron microscopy

ABSTRACT

Electron backscatter diffraction (EBSD) is an automated technique that can measure the orientation of crystals in a sample very rapidly. There are many sophisticated software packages that present measured data. Unfortunately, due to crystal symmetry and differences in the set-up of microscope and EBSD software, there may be accuracy issues when linking the crystal orientation to a particular microstructural feature. In this paper we outline a series of conventions used to describe crystal orientations and coordinate systems. These conventions have been used to successfully demonstrate that a consistent frame of reference is used in the sample, unit cell, pole figure and diffraction pattern frames of reference. We establish a coordinate system rooted in measurement of the diffraction pattern and subsequently link this to all other coordinate systems. A fundamental outcome of this analysis is to note that the beamshift coordinate system needs to be precisely defined for consistent 3D microstructure analysis. This is supported through a series of case studies examining particular features of the microscope settings and/or unambiguous crystallographic features. These case studies can be generated easily in most laboratories and represent an opportunity to demonstrate confidence in use of recorded orientation data. Finally, we include a simple software tool, written in both MATLAB® and Python, which the reader can use to compare consistency with their own microscope set-up and which may act as a springboard for further offline analysis.

1. Introduction

Electron backscatter diffraction (EBSD) is a common laboratory based tool used to measure crystal orientations from crystalline samples. The emergence of the technique can be traced to rapid image analysis routines stemming from both the Yale [1] and Risø [2,3] research labs, which transformed the technique to the heavily automated method we enjoy today. In commercial tools, rapid data acquisition (up to 1200 patterns per second) can be performed with on-line orientation analysis which enables capture of highly detailed maps from very large sample areas.

This pattern analysis is routinely carried out using sophisticated software algorithms to produce extremely rich data sets that can be interrogated for crystallographic texture, grain orientation, grain shape, and local deformation structure. There are several reviews that cover the history of the technique and some examples of its use including a recent review by Wilkinson and Britton [4], as well as excellent reviews by Dingley [5] and Humphreys [6].

In the quest for rapid automation and easy to use software tools it can be difficult to accurately describe the various reference frames for sample orientation and crystal orientation with ease. This difficulty principally concerns the relationship between the indexing step, data recording and beam movement (once around the loop in Fig. 1). This process is repeated for every pattern captured to generate maps for a typical EBSD experiment.

Samples are increasingly being shared between microscopes and labs where different instrument engineers may have established different in-house conventions for these three important steps, often through a simple checkbox during equipment installation, or due to the nature of the SEM environment and detector configuration. These complications, such as choice of scan rotation and beam scan direction, are similar to scan rotation issues found in TEM based techniques such as precession electron diffraction (PED) [7–9]. Further complications are found when using more unusual scanning geometries, such as transmission

* Corresponding author.
E-mail address: b.britton@imperial.ac.uk (T.B. Britton).
[1] Current address: EMPA – Swiss Federal Laboratories for Materials Testing and Research, Laboratory for Mechanics of Materials and Nanostructures, Feuerwerkerstrasse 39, Thun CH-3602, Switzerland.

http://dx.doi.org/10.1016/j.matchar.2016.04.008

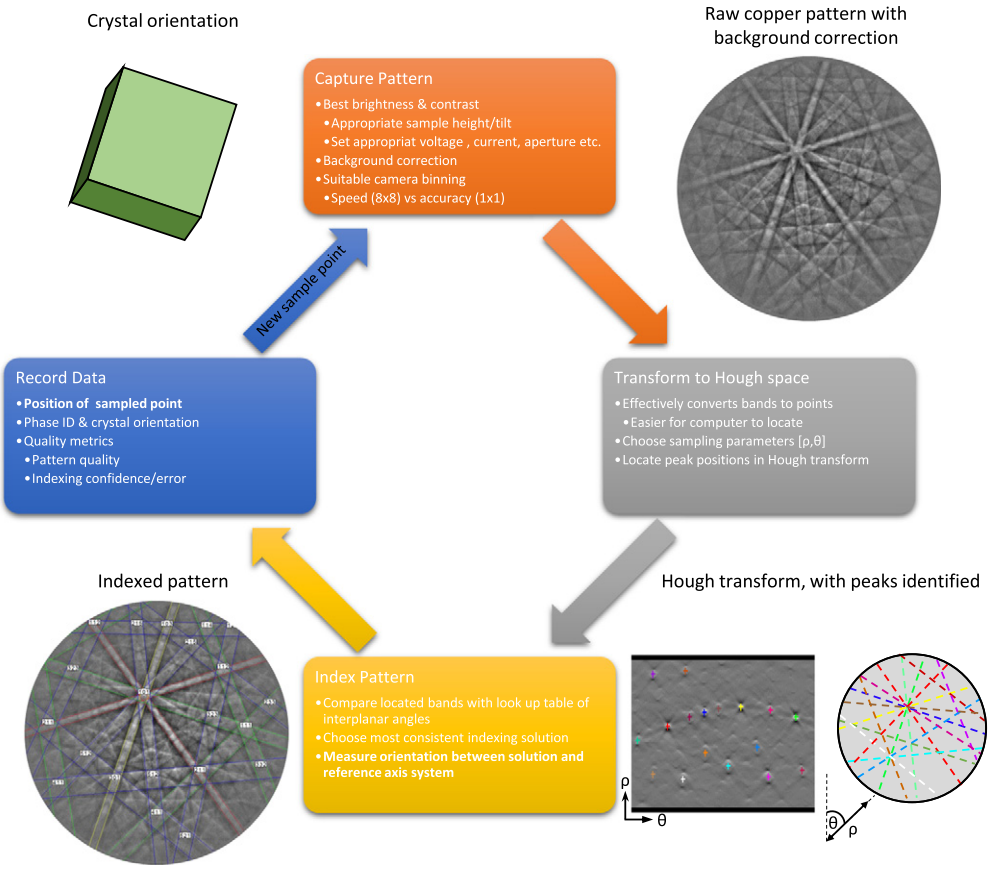

Fig. 1. Overview of EBSD indexing procedure showing pattern capture through to determination of crystal orientation (based upon figure reproduced from [4]).

EBSD (also known as transmission Kikuchi diffraction, TKD) [10,11], or when samples are shared between techniques, such as 3D Laue X-ray diffraction and high resolution EBSD (HR-EBSD) [12]. This problem is also shared when data is used to populate simulations such as crystal plasticity finite element methods [13] or FFT methods [14].

In many cases the convention with which these data are described may be sufficient, as the data is either qualitatively used (such as for grain size estimation or an indication of phase distribution, relative misorientation, or grain morphology), or sample/crystal symmetry renders much of this detail unimportant (such as for texture mapping).

In cases where a precise understanding of the crystal orientation is critical, its determination involves an accurate description of the relation between the sample orientation and mapped crystal orientation, which then allows e.g. the description of the precise grain boundary plane in the coordinate system of the sample. In our experience, the necessary information is often difficult to obtain from the documentation of commercial tools, and the issue can be further complicated by inconsistent appearance of axis systems in the software. Historically, in order to mitigate these problems, individual laboratories have devised test cases that are sufficient for the problem at hand, but may not be universal.

Discussion of our issues with other members of the community reveals that this is a shared concern and this has motivated the current work. Indeed, a recent tutorial paper by Rowenhorst et al. on extending EBSD to 3D volumes highlights this problem [15]. Rowenhorst et al. extend exploration of the problem significantly, in particular in converting between different descriptions of orientation including use of the quaternion, axis angle, and rotation matrices in a more general sense. As a complementary study and for simplicity in this manuscript, we will only use one method of converting from Euler angles to a crystal orientation matrix and demonstrate how this is used to rotate Cartesian vectors. This is expanded and explored in the context of generation of microstructure maps.

In order to regain confidence in accurate descriptions of the crystal orientation, for instance to export data to third party analysis tools, a set of samples and examples are outlined below. This will enable users to exploit conventions where possible, and confidently describe their microscope and orientation convention. We focus on establishing a coordinate system for the diffraction pattern and the convention that the Z axis points out of the sample to establish a consistent set of descriptions for the frames of reference, crystal rotations, and the generation of microstructure maps.

The paper is structured to provide a few key equations and demonstration of a consistent frame of reference which is essential to establish early on. These equations are used to generate a series of conventions, which are suitable for use in our labs but may not be universal. We hope that providing our motivations for these conventions, as well as some simple example code (written in Python and MATLAB®), will be sufficient to convey the ethos of this paper more general. The foundation of this approach is followed by a few case studies that outline validation of our choice in convention, based upon the Bruker convention used in some of our labs, and make its use reproducible in other laboratories when required.

1.1. Frames of reference

Establishing a consistent coordinate frame, with appropriate transformations between the sample, the crystal structure, and the diffraction pattern is at the heart of successful and confident use of EBSD orientation data. Fundamentally there are several 'simple' coordinate systems with respect to different aspects of an EBSD experiment that one could choose.

We start by defining that all coordinate systems used will be right handed, which also implies the right hand rule for the sense of rotations.[2]

[2] This adheres to Convention 1 of Rowenhorst et al. [15].

In principle, the crystal orientations are determined from features in the recorded electron backscatter pattern (EBSP), which is measured as a gnomonic projection of angle-dependent intensities. In the transformation formulas which follow below, we use row vectors which are written here as (x y z) and the transformation matrices thus act from the right. The transformation formulas for column vectors are obtained by using the respective transposed matrix from the left.

A natural choice of coordinate system is based upon the gnomonic projection used to capture the angular diffraction data on a flat phosphor screen, starting with the source point at the electron beam position on the sample, and the central *Z*-axis of the gnomonic projection meeting the detector plane at the point that is called the "pattern centre" (PC). The gnomonic projection transforms polar angles θ into radial distances $\rho = \tan(\theta)$ measured from the pattern centre. This is why, for the detector plane, we define a gnomonic, two-dimensional (X_g, Y_g) coordinate system with (0, 0) at the pattern centre, where (x_g, y_g) are the respective components of the radial distance ρ. We define X_g as pointing right from PC, and Y_g pointing to the top from PC, as seen in Fig. 2A, when viewed with the sample placed behind the screen (as most EBSD cameras are arranged).

The gnomonic coordinate system is defined on the two-dimensional (X_d, Y_d) detection plane in the three-dimensional detector coordinate system (X_d, Y_d, Z_d) in which we measure all distances on a common length scale (pixels, mm, or fractions of the pattern size). The Z_d-axis points from a position on the sample towards the screen and calibrates the gnomonic coordinates via $x_g = x_d/z_d$ and $y_g = y_d/z_d$.

Thus, after calibration of the PC, angular distances $\tan(\theta)$ can be directly measured from the pattern center PC for vectors with polar angle θ away from the Z_d axis. Knowledge of the horizontal and vertical screen size and the relative position of PC on the screen allow us to calibrate the maximum and minimum gnomonic x_g and y_g values in Fig. 2A according to the projection of ρ on these axes.

The relative PC position ($x_g = 0, y_g = 0$) in an EBSP can be described in terms of parameters PC_x, PC_y, and DD, which the Bruker software defines in the following way:

(a) PCx is measured from the left border of the EBSP in units of the pattern width (parallel and in the same direction to X_d in Fig. 2A). This is parallel to our sample tilt axis.
(b) PCy is measured from the top border of the EBSP in units of the pattern height (parallel but in the opposite direction to Y_d in Fig. 2A).
(c) DD as the detector distance L normalised with respect to the pattern height.

Other packages describe the PC position starting from the bottom left of the EBSP instead of the top left as used here. These packages may record this with respect to a square/circular EBSP, illustrating that care must be taken when using rectangular screens, as the aspect ratio of the EBSP is important when converting pattern fractions into effective pixels or mm.

The two-dimensional gnomonic system embedded into the detector system will be used to analyse crystallographically meaningful features that appear in the EBSP, as will shortly be outlined now. Actual parameter conventions and transformation formulas will appear later.

The EBSP is produced from the oriented crystalline region described by a crystal lattice at the origin of the detector coordinate system. The crystal lattice is defined by conventional lattice parameters (a, b, c, α, β, γ).

To conveniently describe the orientation of general, non-orthonormal crystal lattices, we introduce a Cartesian orthonormal system ("standard Cartesian frame"), which will be rigidly fixed to the crystal lattice. For simplicity, we can imagine this Cartesian frame as a small crystalline reference cube that is initially aligned with its (X_c, Y_c, Z_c) axes parallel to the (X_d, Y_d, Z_d) axes of the detector coordinate system. The transformation from the Cartesian basis coordinates to the lattice basis vector coordinates is obtained from the so-called structure matrix $\boldsymbol{A}$ (Eq. (5)).

To fully describe the local orientation of the crystal lattice at the beam spot relative to the detector system, the Cartesian reference frame is rotated from being coincident with the detector system into congruence with the crystal structure of the grain. It is important to note that the Euler angles that appear in the orientation description in the Bunge convention, denote such an "active" rotation of the reference frame basis *vectors*. By virtue of the orthogonality of rotation matrices, the orientation matrix describing this reference system rotation also provides the "passive" *coordinate* transformation of a fixed vector from the unrotated into the rotated system.[3]

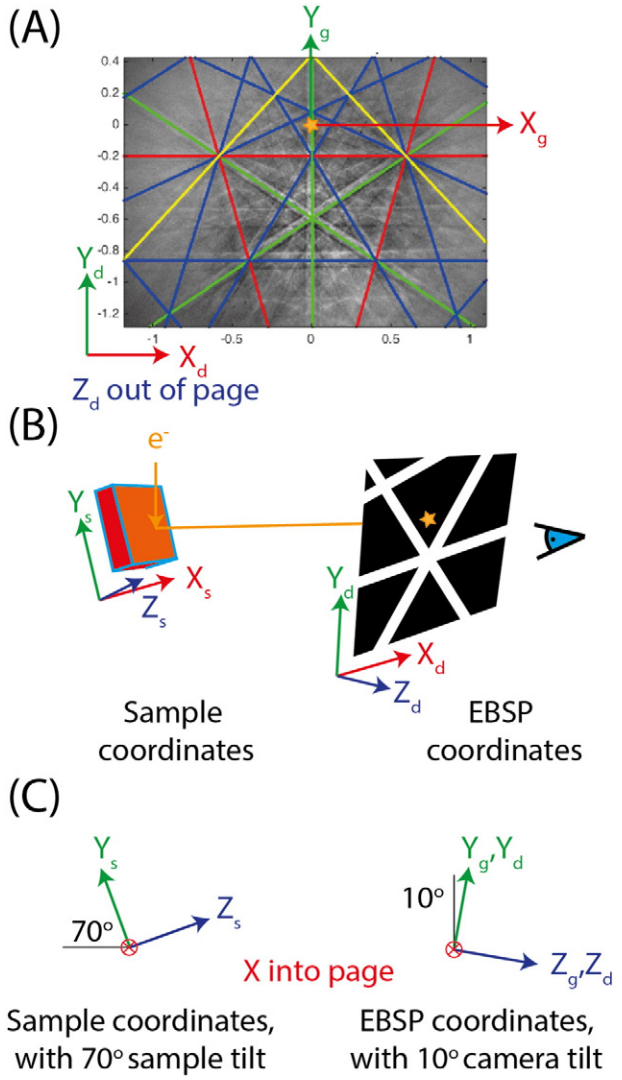

Fig. 2. Frames of reference for EBSD analysis, all of which are right handed: (A) definition of a right handed frame within the diffraction pattern, with (0,0) located at the pattern centre (as indicated with an orange star), X pointing from left to right, and Y pointing from bottom to top; (B) rendering of observation of the EBSP with respect to a sample inserted into a SEM chamber, where Z and Z point out of the page; (C) transformation between the sample and EBSP coordinates with only a rotation about the X axis.

[3] For a general transformation matrix of the basis *vectors*, the respective *coordinate* transformation from the "old" into the "new" system is given by the transpose of the inverse matrix. This subtle difference is easily overlooked since the inverse of the transpose of a rotation matrix is the initial matrix itself. The Bunge convention explicitly describes the active, "rigid body" rotation of the three basis vectors, by which the passive coordinate transformation is then implied. Accidentally, this specific coordinate transformation involves the same rotation matrix, however, with a different interpretation.)

As will be shown below, the overall transformation from the detector system to the crystal lattice can be split into three basic conceptual steps:

1) Start with the standard Cartesian frame aligned with the detector frame and bring it into coincidence with the sample coordinate system by a rotation $\boldsymbol{R}_{x(\alpha)}$ (Eq. (9), Eq. (16), and Eq. (17)). This will define the null position of the Euler angles.
2) Rotate the Cartesian standard frame from this detector-independent reference position into coincidence with the frame of the local lattice. This rotation $\boldsymbol{O}$ will define the orientation of the grain under investigation by the Euler angles, measured in the specimen frame of reference established in step 1. In this way, the orientation data obtained by EBSD can be compared with the results from alternative techniques.
3) Transform the rotated Cartesian basis vectors to the crystal lattice basis vectors using the structure matrix $\boldsymbol{A}$ (Eq. (5)).

This shows that, for an independent determination of the grain orientation $\boldsymbol{O}$, we need to define a convention for the structure matrix $\boldsymbol{A}$, and we need to calibrate the transformation $\boldsymbol{R}_{x(\alpha)}$ from the detector system to the sample system.

In order to extract the orientation $\boldsymbol{O}$ from the combined action of all three steps discussed above, in principle, one needs to identify the position of crystallographic features (lattice plane traces and zone axes) appearing in the gnomonic system of the Kikuchi diffraction pattern ("index the pattern"). This defines an observed total coordinate transformation from the crystal coordinates ($u_k\ v_k\ w_k$) to the detector coordinates ($x_d\ y_d\ z_d$), in which $\boldsymbol{O}$ is implicitly included. Both sets of coordinates refer to the same direction but are described in different reference systems. Finally, in the EBSP, the fixed direction ($u_k\ v_k\ w_k$) will be found at gnomonic coordinates $x_g = x_d/z_d$ and $y_g = y_d/z_d$. We see that it is central to this procedure to be able to transform vector coordinates between the systems which are linked by transformation matrices (which are also defined according to specific conventions).

This qualitative discussion outlines the importance of correctly linking the different frames of reference and their coordinate systems, notably:

g — 2D gnomonic projection system of the EBSP with the ($x_g = 0$, $y_g = 0$) at PC_x, PC_y.
d — Detector system with $z = 0$ on the sample, i.e. at the beam position, a distance DD away from the screen.
s — Sample system, with the 2D EBSD map system as the X_s-Y_s-plane of the specimen.
c — Cartesian standard frame of the crystal, defined in a fixed relation to the crystal lattice k.
k — Bravais or crystal lattice, defined by Fig. 4 and Eqs. (1)–(4), (see later).

Unfortunately a poor description and validation of conventions used for the coordinate systems and the transformation matrices lead to improper, or even wrong, interpretation of the crystallographic orientations reported by EBSD. This motivates our choice of experiments, associated mathematical descriptions and example MATLAB® and Python codes as described next.

1.2. Frames of reference — sample

Linking of an electron micrograph, or map of scanned points, to the sample coordinate system *S* needs the precise scanning locations of the beam to be mapped for a particular instrument and camera. This frame of reference needs to be expressed in a form that is useful to the scientist and we aim to establish a 'natural' sample frame that lies on the sample surface (see Fig. 2B).[4]

[4] Furthermore, any EBSD user must be careful when exchanging images between software as many computer graphics software packages will use a 'top left' origin, while the natural frame scientists often adopt is a 'bottom-left' origin (these are often called 'ij' and 'xy' coordinate systems respectively).

One way to explore the relationship between the mapping position of the electron beam and the detector system is to measure the systematic changes in the PC which are caused by the movement of the beam relative to the detector screen. This PC movement is routinely measured by the EBSD software packages, as an accurate PC is required to accurately describe the crystal orientation for large area maps. Typically PC measurement is performed through optimisation of the best PC to maintain the angles between recorded planes. Furthermore, correlation between the SEM image and the EBSP can be confirmed through direct tracking of features moving within patterns captured.

To reduce ambiguity due to the choice for PC_y (in the Bruker software PC_y is counted from the top of the recorded EBSP), we will only use the systematic variations in detector distance DD, describing the distance between interaction volume and EBSD phosphor screen, and variations in PC_x to validate our choice of convention. Changes in DD are readily apparent as a change in 'zoom' of the pattern (magnification increases as the detector is retracted away from the sample).

Validation of the relationship between the EBSP axes system and a mapped area can be performed using a simple large area map of a single crystal of undeformed silicon wafer. As the crystal orientation of this sample does not change, scanning a large area only results in movement of the PC.

A map spanning 3000 μm in X and 2200 μm in Y was performed using a Zeiss Auriga-40 SEM equipped with Bruker ESPRIT 1.9. The sample was tilted to the EBSD configuration using the stage (a tilt about the sample X_S axis). The sample was scanned using tilt correction in the Zeiss SmartSEM software and no scan rotation correction was employed.

The movement of the PC is shown schematically in Fig. 3A. Four points are indicated and their relative expected positions within a map are indicated:

1) The top left of the sample — a long detector distance and a small value of PC_x.
2) The top right of the sample — a long detector distance and a large value of PC_x.
3) The bottom right of the sample — a short detector distance and a large value of PC_x.
4) The bottom left of the sample — a short detector distance and a small value of PC_x.

Note that these four points have been chosen to run clockwise when looking down the negative Z axis towards the sample.

Fig. 3B reveals that the detector distance and PC_x measurements with respect to the beam X and beam Y positions are rotated 180° about the Z_s axis with respect to the EBSP coordinate system, in order that the numbered coordinates match the expected PC positions. This is highlighted in Fig. 3C. This rotation of 180° about Z_s maintains a right hand set. This creates a sample coordinate system that can be overlaid on maps of EBSD measurements, indicated in Fig. 3C, which is different to beam positions as noted within associated coordinate files (e.g. ".ctf" or ".ang" files) and therefore requires care when establishing a position grid from a captured map if the data is to be processed by third party software/code.

The orientation of our sample system corresponds directly to the "global" system suggested by Jackson et al. [16] for use in an open data format for EBSD.

2. The unit cell

Linking the EBSP to the orientation of a unit cell is greatly simplified by defining a Cartesian reference frame for the crystal lattice. This enables rapid and consistent transformation between the crystal lattice and a right handed orthonormal coordinate system.

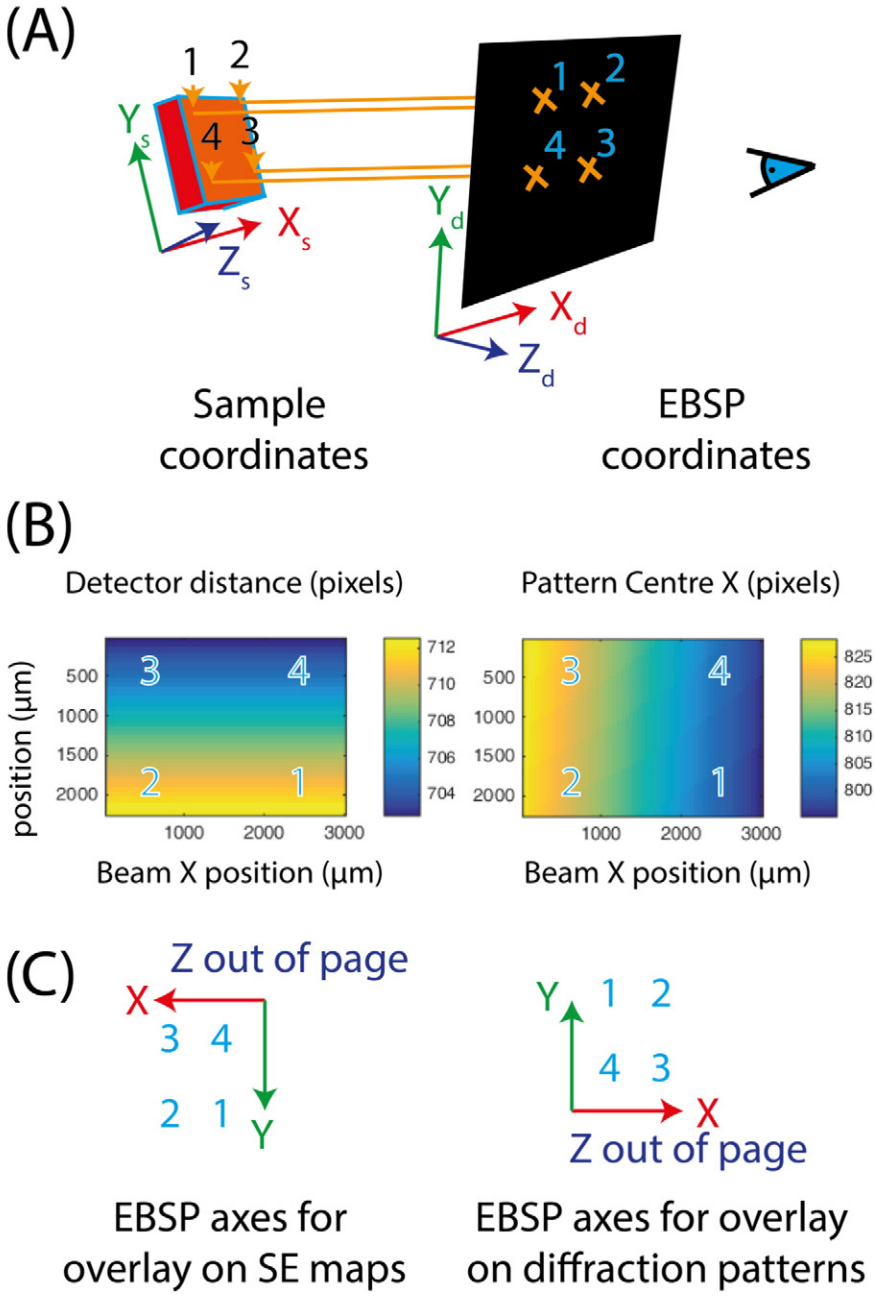

Fig. 3. Relationship between the scanning coordinates and the EBSP coordinate system, as described in Fig. 2. (A) The position of the pattern centre for four mapped points on a sample, with X_s and Y_s representing a 'natural' choice of sample coordinate frame and where the Y_s axis points 'up' the sample; (B) variations in detector distance and pattern centre X for a scanned map, following the beam X and Y position convention to represent the map, with colours indicating position in pixels; (C) the relationship between the EBSP axes and a scanned image (e.g. SE image). Note the 180° rotation about the Z axis required.

The unit cell is commonly described using three lengths, a, b and c and three angles α, β, γ. α describes the angle between the b and c axes, β between c and a, and γ between a and b. These values describe a primitive unit cell with lattice vectors **a** **b** and **c**.

In principle, the reference crystal lattice can be oriented arbitrarily in the Cartesian reference system. However to ensure meaningful data and consistency, we assume a convention (shown in Fig. 4) which leads to:

- **a** **b** and **c** form a right handed set.
- **c** is parallel to the Z_C axis.
- **b** lies in the y_C–z_C plane, at an angle α to **c**.
- **a** is pointed such that it is an angle β to **c** and γ to **b**.

This convention [17] results in the following algebraic descriptions of the reference crystal base vectors in the Cartesian frame for a general triclinic lattice:

$$f = \sqrt{1-\cos\alpha^2-\cos\beta^2-\cos\gamma^2+2\cos\alpha\cos\beta\cos\gamma} \quad (1)$$

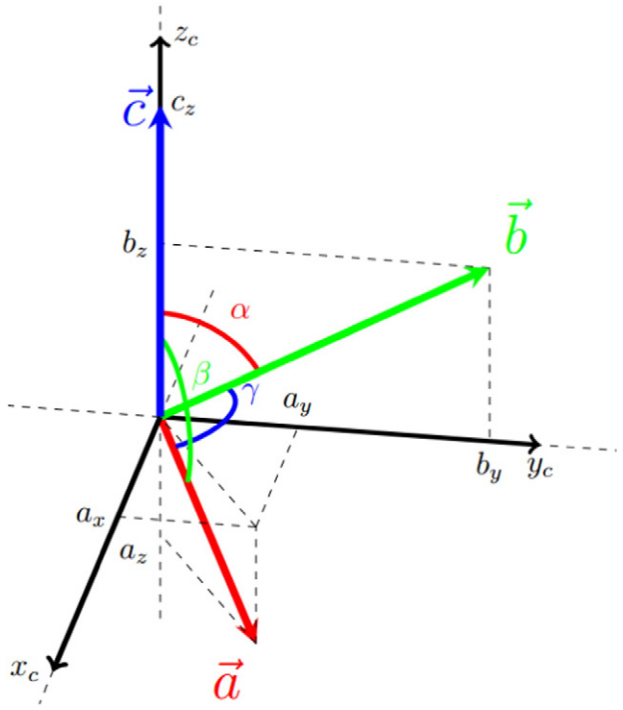

Fig. 4. Pictorial representation of the unit cell convention (as described by Eq. (5)).

$$\boldsymbol{a}_c = a\left(\frac{f}{\sin\alpha} \quad \frac{\cos\gamma - \cos\alpha\cos\beta}{\sin\alpha} \quad \cos\beta\right) \tag{2}$$

$$\boldsymbol{b}_c = b(0 \quad \sin\alpha \quad \cos\alpha) \tag{3}$$

$$\boldsymbol{c}_c = (0 \quad 0 \quad c). \tag{4}$$

For calculations, it is useful to describe the transformation of the Cartesian unit column vectors to the coordinates of the lattice base vectors by the structure matrix, $\boldsymbol{A}$:

$$\boldsymbol{A} = \begin{pmatrix} a\frac{f}{\sin\alpha} & 0 & 0 \\ a\frac{\cos\gamma - \cos\alpha\cos\beta}{\sin\alpha} & b\sin\alpha & 0 \\ a\cos\beta & b\cos\alpha & c \end{pmatrix}. \tag{5}$$

The structure matrix enables the coordinate transformation from the crystal lattice to the Cartesian system c for direct lattice $(uvw)_k$ row vectors, using the transpose of $\boldsymbol{A}$, (i.e. $\boldsymbol{A}^{\boldsymbol{T}}$):

$$(u_c \quad v_c \quad w_c)_c = (u \quad v \quad w)_k \boldsymbol{A}^{\boldsymbol{T}}. \tag{6}$$

In a similar form, the structure matrix can be used to transform from the reciprocal crystal lattice k^* to the reciprocal Cartesian system c^* for row $(hkl)_{k^*}$ vectors, using the inverse of $\boldsymbol{A}$, (i.e. $\boldsymbol{A}^{-1}$):

$$(h_c \quad k_c \quad l_c)_{c^*} = (h \quad k \quad l)_{k^*} \boldsymbol{A}^{-1}. \tag{7}$$

The convention for the crystal unit cell (i.e. the population of the structure matrix) can have significant impact on how crystal orientations are described, both numerically and geometrically. For example, different commercial manufacturers of EBSD systems have differing default conventions which can be seen in mapping hexagonal close packed (HCP) materials, where the reference crystal as described by one manufacturer is different from another by 30° (translating conventions between manufacturers have been explored previously, such as in texture analysis of welds by Fonda et al. [18]). In the convention described here, a hexagonal cell ($\alpha = \beta = 90°, \gamma = 120°$) will have the Y axis parallel to an <a> direction and the Z axis is parallel to the <c> direction. In the same way, the unit cell settings and atomic coordinates in crystallographic databases can vary. Both of these must be carefully considered when comparing experimental results between different measurement systems or techniques.

Furthermore, we note that convention introduced here is different from often used conventions for monoclinic systems, where the unique axis is placed along the **b** axis (instead of **c**). If this is desired, then the relevant Miller indices can be transformed using a cyclic change of indices [19].

3. Orientation

A crystal orientation $\boldsymbol{O}$ can be defined by an active rotation which brings the set of Cartesian basis vectors (Eqs. (1)–(4)) into coincidence with the Cartesian test frame associated with the crystal lattice, starting from the reference position parallel to the sample system. The respective orientation matrix can be constructed from a series of ordered rotations parameterised with Euler angles, where each Euler angle describes a rotation about a characteristic axis. An arbitrary rotation can be based upon two rotation matrices:

$$\boldsymbol{R}_z = \begin{pmatrix} \cos\theta & \sin\theta & 0 \\ -\sin\theta & \cos\theta & 0 \\ 0 & 0 & 1 \end{pmatrix}. \tag{8}$$

$$\boldsymbol{R}_x = \begin{pmatrix} 1 & 0 & 0 \\ 0 & \cos\theta & \sin\theta \\ 0 & -\sin\theta & \cos\theta \end{pmatrix}. \tag{9}$$

The Bunge convention for orientations [20] uses the transformation matrices defined above to construct an orientation matrix via matrix multiplication in which each successive transformation left multiplies the previous one in a ZXZ-axis sequence:

$$\boldsymbol{O} = \boldsymbol{R}_{z(\phi_2)}\boldsymbol{R}_{x(\Phi)}\boldsymbol{R}_{z(\phi_1)}. \tag{10}$$

The order of operations described in Eq. (10) means that all three Cartesian basis vectors are first rotated ϕ_1 about Z, followed by Φ about the new X axis, followed by ϕ_2 about the updated Z axis. The rotation matrix $\boldsymbol{O}$, acting on fixed *column* vectors in the unrotated system, also gives the new coordinates of a fixed vector with respect to the rotated basis (a passive rotation).[5]

Acting on *row* vectors from the right, the rotation matrix $\boldsymbol{O}$ described in Eq. (10) transforms the Cartesian coordinates of a vector $\boldsymbol{u}_c$ from the rotated system back to the coordinates $\boldsymbol{u}_s$ in the unrotated sample system s:

$$\boldsymbol{u}_c = (u_x \quad v_y \quad w_z)_c. \tag{11}$$

$$\boldsymbol{u}_s = \boldsymbol{u}_c\boldsymbol{O}. \tag{12}$$

A combination of the operations defined so far can be used to describe the conversion of the coordinates of a direction, *uvw*, from the crystal into the sample frame of reference:

$$(x \quad y \quad z)_s = (u \quad v \quad w)_k \boldsymbol{A}^{\boldsymbol{T}}\boldsymbol{O} = (u \quad v \quad w)_k \boldsymbol{G}_{sample}. \tag{13}$$

Similarly, the rotation of a crystal plane with reciprocal lattice coordinates *hkl* into the reciprocal sample frame of reference can be

[5] Note that this is not the definition of the orientation in the Bunge convention, but rather a result following from that definition.

performed:

$$(x^* \quad y^* \quad z^*)_s = (h \quad k \quad l)_k \boldsymbol{A}^{-1}\boldsymbol{O}. \tag{14}$$

Inversion of Eq. (13) can be used to obtain the crystal lattice coordinates $\boldsymbol{u}_k = (u \quad v \quad w)_k$ of a fixed crystallographic feature that is known in the sample frame:

$$(u \quad v \quad w)_k = (x \quad y \quad z)_s \boldsymbol{O}^{\boldsymbol{T}} \boldsymbol{A}^{\boldsymbol{T}^{-1}}. \tag{15}$$

Here we note that the use of $\boldsymbol{A}^{\boldsymbol{T}}$ and $\boldsymbol{A}^{\boldsymbol{T}^{-1}}$ must be considered with significant care, as this is not necessarily an orthogonal matrix. However $\boldsymbol{O}$ is a rotation matrix and therefore $\boldsymbol{O}^{\boldsymbol{T}}=\boldsymbol{O}^{-1}$ which disguises the need for inversion in Eq. (15). This can lead to confusion in connection with non-orthogonal matrices like $\boldsymbol{A}$, which again emphasizes the need for consistent definitions. We note that Eq. (15) can clearly be extended beyond vector transformation towards higher rank tensors as needed.

The actual coordinate systems and rotation axes are likely to be different for different EBSD software and hardware vendors and tools. We have chosen to follow the convention used within the Bruker ESPRIT software (see later), and it is likely to be different for different software vendors and tools. Use of different conventions can represent complications when common data structures (such as ".ang" or ".ctf" files) are used without an appropriate numerical example or header file describing the convention employed (this must include scan axis system and rotation convention).

3.1. Relationship between the EBSP coordinate system and the sample

In the simplest case, transformation from the detector coordinate system, containing the EBSP, to the coordinate system of the sample is assumed to involve a tilt about the X_s axis. Typically, EBSD cameras are inserted at a slight angle into the chamber and the sample is tilted. Therefore the effective rotation angle, α, can be calculated from a combination of the camera tilt angle, $\theta_{detector}$, and the sample tilt, θ_{sample}:

$$\alpha = (\theta_{sample} - 90^\circ) - \theta_{detector}. \tag{16}$$

If the reference crystal, with Euler angles (ϕ_1=0, Φ=0, ϕ_2=0), is in the sample frame of reference (with the appropriate choice of origin and sense for mapped coordinates with respect to sample coordinates, as shown in Fig. 3) then the rotation from the sample to the detector can be performed using a further rotation about X_s if the sample coordinate system is aligned such that the X_s axis of the specimen is co-linear with the X_d axis of the detector frame. The crystal coordinates in the detector frame are then obtained via:

$$(x \quad y \quad z)_d = (u \quad v \quad w)_k \boldsymbol{A}^{\boldsymbol{T}} \boldsymbol{O} \boldsymbol{R}_{x(\alpha)} = (u \quad v \quad w)_k \boldsymbol{G}_{detector}. \tag{17}$$

3.2. Validation of conventions

Several case studies will be used to demonstrate that the chosen conventions are consistent and useful in describing crystal orientations of materials.

Example 1. — rotation of a single crystal.

In most SEMs a rotation of a single crystal using an in-plane crystal rotation is trivial to perform in the chamber when the sample is tilted using the stage tilt axis. This is a very useful test to check whether the sense of rotation is maintained between the secondary electron (SE) map and the EBSP. A deformed single crystal of Ni-based superalloy was scanned and pattern captured (Fig. 5). The sample imaged containing two specks of dust which act as fiducial markers.

Comparison of the SE images, rotated by 180° as per the convention established in Fig. 3, and the EBSP reveal that a clockwise rotation of the sample is consistent with a clockwise rotation of the pattern approximately about the sample normal. This confirms that both mapping of the sample and the EBSP have the same handedness, such that we are viewing the EBSP from the viewpoint illustrated in Fig. 2B and Fig. 3A. Note that the 180° correction is not needed for this test to be passed,

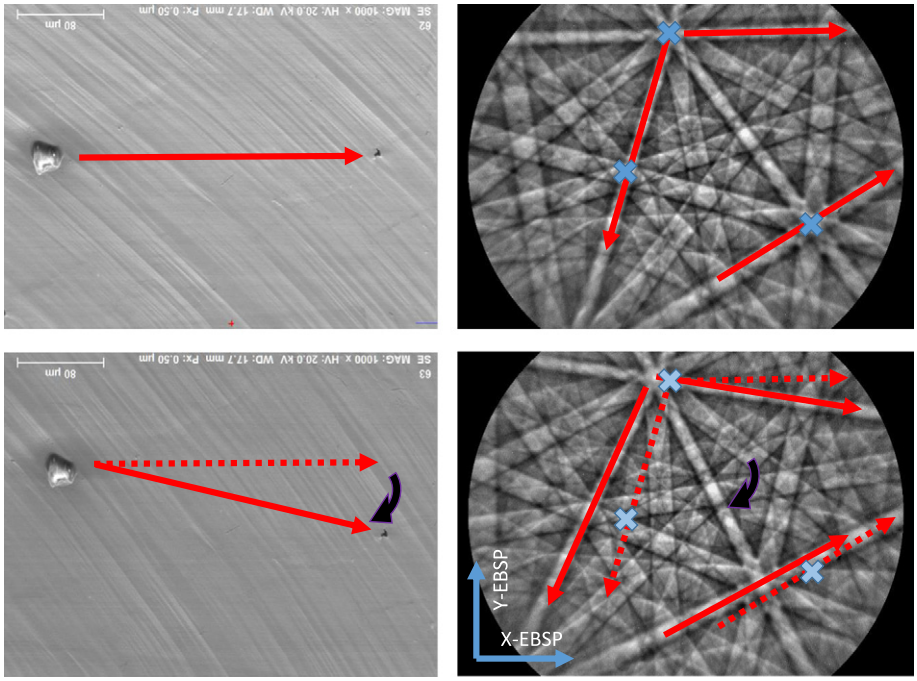

Fig. 5. Rotation of a single crystal Ni-superalloy sample: (left) SE images; (right) EBSPs. Both SE images and EBSP rotate clockwise (top row as compared with bottom row). Rotation of the SE image is rotated from the captured image to reflect the 180° rotation required, as demonstrated in Fig. 3.

as instead it only tests the handedness of the applied and measured rotations.

Example 2. — confirmation of cubic twin planes in 3D.

The subsurface inclination of the crystal can be important, especially when using EBSD data to precisely inform crystal plasticity simulations or extracting out of plane materials properties. Surface trace analysis, e.g. of slip bands or coherent twin interfaces, is insufficient to describe the inclination of planes with respect to the sample. Instead subsurface information is required.

A sample of polycrystalline Ni-based superalloy was selected as it has many coherent $\sum 3$ boundaries due to the presence of annealing twins, as Ni has a low stacking fault energy. The $\sum 3$ boundary describes a boundary where the ABC-ABC stacking of the crystal is interrupted to give a CAB-C-BAC type stacking of the crystal lattice. This can be described in terms of a 60° rotation about the <111> crystal axis. For a coherent twin, this orientation relationship is supplemented by the boundary plane lying on a {111} plane. This motivates the use of a twinned FCC material with many coherent annealing twins as a calibrant for the 3D orientation relationship between EBSP and mapped coordinate system using the twin habit plane as confirmation. These are readily available (e.g. oxygen free high conductivity copper or nickel) and many twins are readily observed. The coherent boundaries are long and straight.

Confirmation of the twin relationship can easily be performed through analysis of pole figures from the twin and the parent grains obtained using EBSD. Plotting of the shared orientation relationship components (e.g. twin plane normal or rotation axis) will reveal a shared point between pole figures from twin and parent. In the case of FCC materials the traces of the twin habit plane on the top and subsurface planes should be consistent with the {111} twin system (for a $\sum 3$ twin). This analysis on its own confirms that the misorientation relationship between examined points within a map is consistent. Subsequent analysis of a microstructural feature with respect to the crystallographic twin relationship can be used to confirm the relationship between sample and EBSP.

Measurement of the sub-surface inclination of the twin habit plane can be performed using focussed ion beam (FIB) sectioning and subsequent EBSD analysis (i.e. keeping the twin sub-section and the EBSD in the same frame of reference). In this case, FIB sectioning was performed using Ga^+ ions on the Zeiss Auriga-40 FIB-SEM cross beam platform. A twin was identified in the secondary ion induced SE image, due to strong ion channelling. Note that imaging with the ion beam damages the crystal lattice (due to Ga^+ ion implantation, but this lattice is relatively robust).

One grain was selected that contained more than one twin with surface traces at an angle to the Y axis of the SE map. This is important as it enables a small trench cut, normal to the sample surface and parallel to the tilt axis to be made, so that the subsurface twin boundary could be examined using SE channelling just prior to an EBSD map.

Once the trench was cut, the sample was moved and tilted to the EBSD condition and imaged to generate a SE image that showed the subsurface direction of twin habit plane. Tilt correction was performed for the top surface at 70° for EBSD analysis (i.e. the cross section plane is stretched oddly and so precise interpretation of the angles is not trivial). A SE image was captured within the EBSD software (ESPRIT 1.9) and the EBSD mapping performed immediately afterwards, avoiding any ambiguity in interpretation of the sub-surface twin inclination, but not necessarily generating the strongest contrast for the cross section image.

An overlapping SE image and inverse pole figure map is shown in Fig. 6A. A schematic of the interrogated volume is shown in Fig. 6B, where the inclination of the sub-surface twins can be seen with faint contrast in the trench part of the SE image in Fig. 6A (note that this contrast could either be slight surface relief or electron channelling, and that either contrast mechanisms are sufficient to describe the subsurface inclination of the boundary).

Fig. 6C demonstrates that a crystallographic analysis of the shared twin planes confirms that the surface traces are consistent with the surface traces shown in Fig. 6A. This analysis involves the intersection of a plane in 3D with the surface normal which results in a direction that lies on a zone perpendicular to the line connecting the plane normal and the surface normal within a stereographic projection. This surface trace analysis would be correct with or without a 180° correction for the relative alignment of the X-Y-Z axes of both pole figure and orientation map.

Analysis of the subsurface inclinations of the habit plane, highlighted with arrows in Fig. 6D, confirms that for the pole figure to be consistent with the mapped coordinate grid, the complete pole figure drawing must be rotated by 180° which is consistent with the analysis presented in Fig. 3.

Example 3. — consistent plotting of unit cell, pole figures and EBSPs.

This example uses computer code to take Euler angles as described by the Bruker ESPRIT package to generate an EBSP using a gnomonic

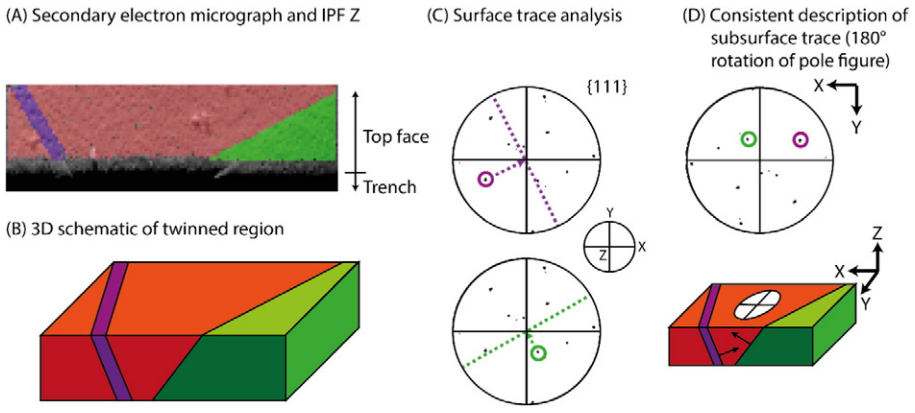

Fig. 6. Analysis of a twin habit plane to confirm that a 180° rotation about Z is required to map the crystallographic data to the SE image. (A) SE & IPF map showing the twin arrangement, including the subsurface inclination; (B) a 3D schematic of the twinned grain; (C) pole figures are generated using ESPRIT 1.9 with the common {111} habit plane highlighted as a member of the dashed zone, only poles in the positive hemisphere are shown; (D) rotation of the pole figure by 180° to match inclination of the sub-surface traces.

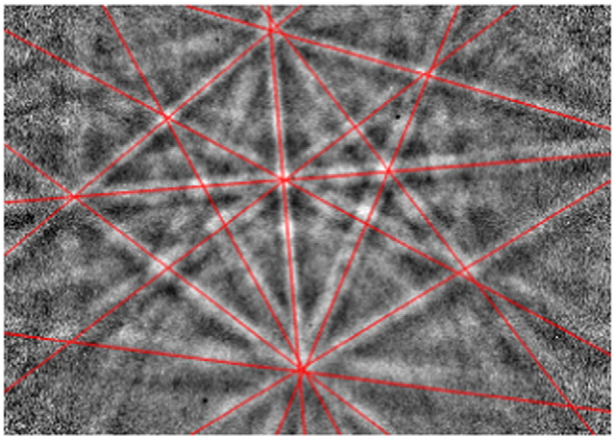

Fig. 7. Example EBSP from a Ni superalloy, captured on an e$^-$ FlashHR EBSD detector with a 20 kV accelerating voltage and measured using ESPRIT 1.9. A slight degradation of the pattern is due to ion beam damage from FIB trenching nearby.

projection in the EBSP coordinate system and spherical projection, combined with a unit cell in both the sample and EBSP coordinate systems, and pole figures in the sample coordinate system. The code can be modified for other EBSD measurement systems and is attached for use by the reader (in MATLAB® and Python forms).

A diffraction pattern from Ni was captured for analysis. The system was calibrated in Bruker ESPRIT 1.9. The detector was tilted to 4.6° and the sample was tilted to 70°. The crystal orientation was measured as Euler angles: ($\phi_1 = 127°, \Phi = 38°, \phi_2 = 273°$). The PC, in Bruker coordinates, was measured as: [$PC_x = 0.48, PC_y = 0.28, DD = 0.64$] with a pattern aspect ratio of 1.39 (width/height).

The Ni crystal diffraction pattern was simulated with cubic symmetry (i.e. $\alpha = \beta = \gamma = 90°$, and $a = b = c = 0.361$ nm). We follow the conventions described in Eqs. (1)–(19) to use these values and generate a diffraction pattern. The position of bands on the screen was calculated for the {111}, {200}, {220}, and {311} families of planes.

The position of a band on a screen using a gnomonic projection can be described as a line that goes between two points, P_1 and P_2, where the PC is (0,0,DD). For the creation of the simulated EBSP showing the geometry of the diffracting planes in the gnomonic projection, we used the properties of the Hesse normal form of lines and planes to obtain the intersection of a plane with a normal vector, $n = (n_x, n_y, n_z)$ originating from (0,0,DD) and the screen:

$$\chi = \mathrm{a}\tan\left(\frac{n_y}{n_x}\right) \tag{18}$$

$$\theta = \mathrm{a}\cos(n_z) \tag{19}$$

$$R_{gnomonic} = \tan\theta \tag{20}$$

$$d_{Hesse} = \tan\left(\frac{\pi}{2} - \theta\right) \tag{21}$$

$$\alpha_{Hesse} = \mathrm{a}\cos\left(\frac{d_{Hesse}}{10}\right). \tag{22}$$

Two points that sit on a circle (of radius 10 in pattern fractions, i.e. extending far beyond the screen dimensions) within the gnomonic projection, away from the PC with angles α_1 and α_2 are:

$$\alpha_1 = \chi - \pi + \alpha_{Hesse} \tag{23}$$

$$\alpha_2 = \chi - \pi - \alpha_{Hesse}. \tag{24}$$

The points in the plane of the phosphor are therefore:

$$P_1 = 10[\cos(\alpha_1), \sin(\alpha_1)] \tag{25}$$

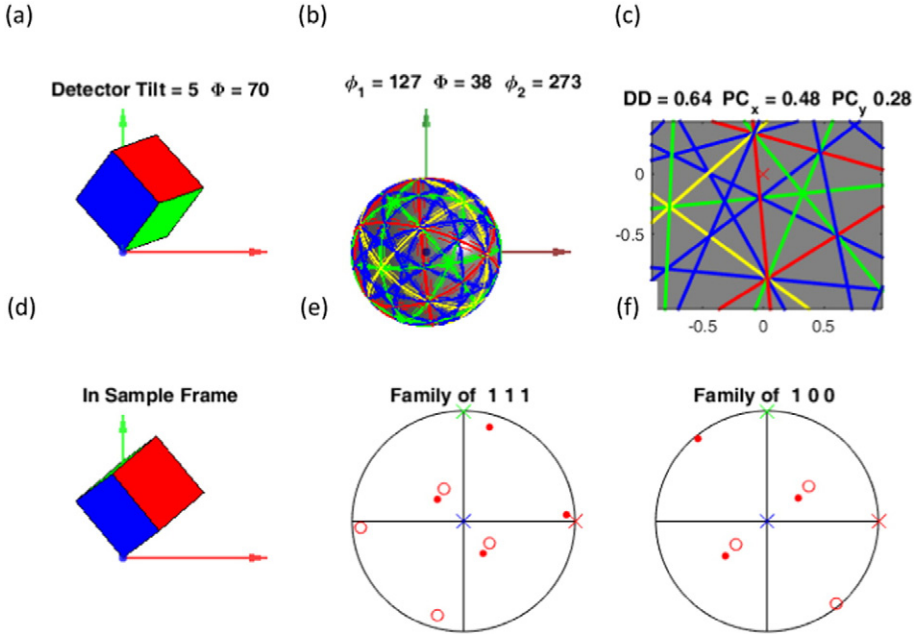

Fig. 8. Simulation of the electron diffraction pattern shown in Fig. 7 with the gnomonic projection (c) and spherical projection (b), as well as the unit cell in the (a) detector and (d) sample frames of reference. The pole figures show (e) the {111} and (f) {100} families of planes, with filled symbols indicating directions pointing to the northern hemisphere and the hollow symbols pointing to the southern hemisphere. The arrows for the spherical projection and unit cells, as well as the coloured crosses in the pole figures indicate the reference axes directions which form a right handed set and [X = red, Y = green, Z = blue].

$$P_2 = 10[\cos(\alpha_2), \sin(\alpha_2)]. \quad (26)$$

Plotting these two points for each reflection is sufficient to generate a plot of the band centres and represents the geometry of the underlying diffraction pattern.

Representation of the diffraction pattern shown in Fig. 7 is demonstrated in Fig. 8. The simulated pattern accurately captures the precise location of the diffracting planes in the EBSP frame of reference.

Accurate reproduction of the gnomonic projection can be verified through comparison of a spherical projection and the simulated EBSP (an explicit description of this projection is provided in the Python and MATLAB® codes). Generation of the unit cell in the detector frame of reference is consistent, as the yellow diffraction planes are the {200} which are represented appropriately.

The {111} pole figure shown in Fig. 8 is one of the points shown within the pole figures reported in Fig. 6. This is the green twin system, illustrating consistency between this code and representation of object morphologies in the sample frame of reference.

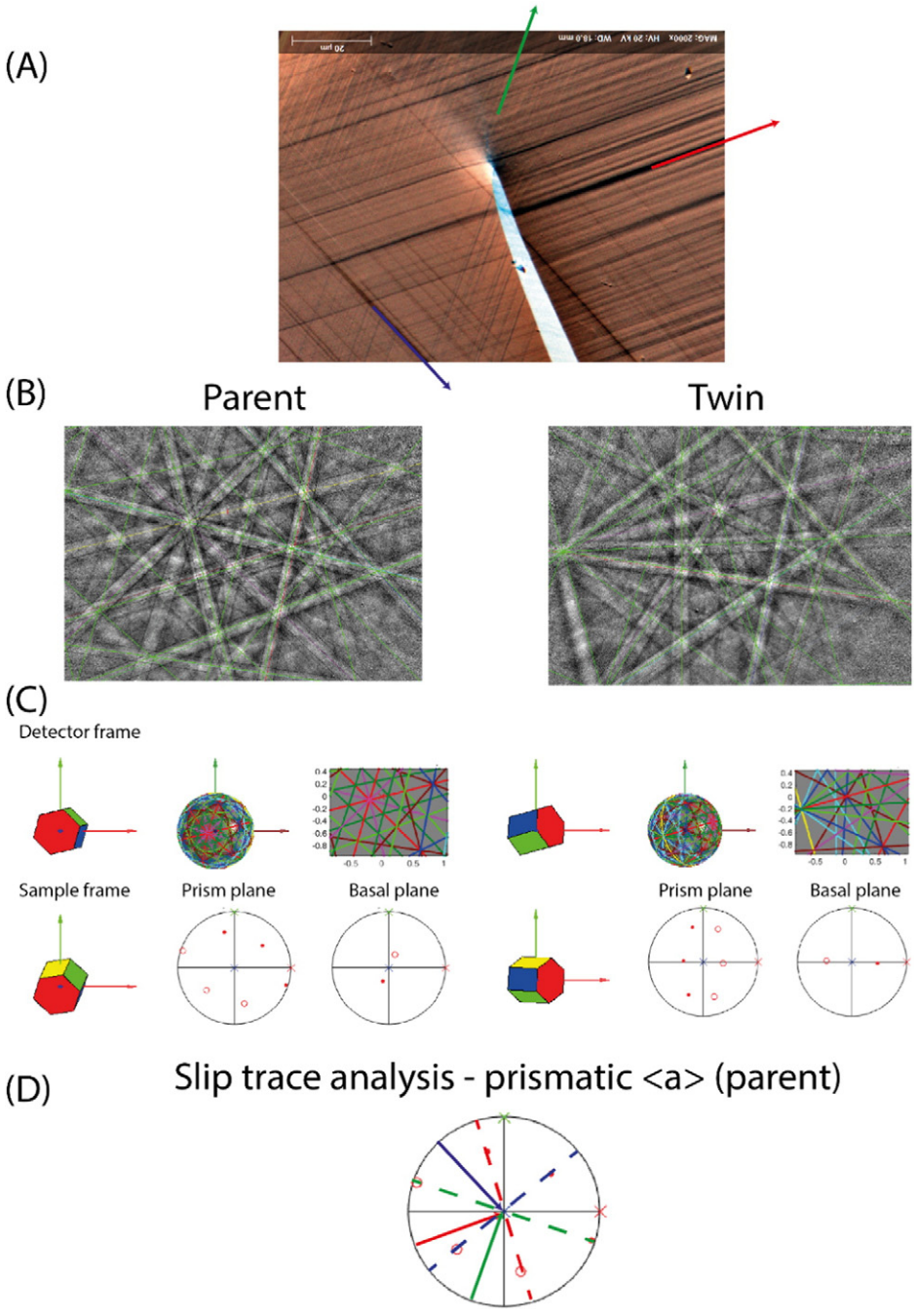

Fig. 9. Confirmation of crystal orientations and slip trace analysis for deformation in commercially pure titanium: (A) Argus forescatter image showing slip bands and the deformation twin; (B) example diffraction patterns; (C) demonstration that simulated patterns and crystal orientations match the twin and parent orientations; (D) slip trace analysis confirming that the prominent slip bands in (A) are from <a> prismatic slip in Ti. Arrows indicate the directions of the surface traces, as highlighted in (A), and the dashed lines overlap with each of the prism planes.

MATLAB® code for generation of this figure is included in the supplementary information and Python code for generation of the simulated EBSP is also included for completeness.

Example 4. — slip band identification in a lower symmetry material.

Examples 1–3 so far have focussed on cubic crystals. The 24 symmetry operators commonly found in cubic materials may hide some important details when precisely describing crystal orientations. For instance, one of these is the choice of convention for the <a>, <b> and <c> with respect to the reference frame (described formally using Eq. (1) to Eq. (4)). If validation is performed exclusively against a cubic crystal then this is not sufficient for general understanding of a system of rotations and unit cell conventions.

This example extends our analysis to a hexagonal closed packed material, specifically commercially pure titanium, and accurately simulates the geometry of a diffraction pattern. The crystal orientation reported is used to identify physically reasonable slip bands for the active slip system, observed near a deformation twin.

The sample was measured in a Zeiss Merlin equipped with a Bruker e$^-$ FlashHR and ESPRIT 1.9 software. Image tilt correction was used on the Zeiss SmartSEM software and no image rotation was applied. The scanning coordinate system of this instrument was confirmed to be similar to the Zeiss Auriga instrument used for other case studies presented in this paper.

The PC for this map was: $[PC_x = 0.44, PC_y = 0.71, DD = 0.71]$. The detector was tilted to 4° and the sample was tilted to 70°. The crystal orientation of the parent was measured as: $(\phi_1 = 337°, \Phi = 29°, \phi_2 = 5°)$; and the twin as $(\phi_1 = 87°, \Phi = 50°, \phi_2 = 270°)$. The titanium crystal was simulated with $\alpha = \beta = 90°$, $\gamma = 120°$, and $a = b = 0.295$ nm, $c = 0.468$ nm. Reflectors of: {1-10}, {002}, {1-11}, {1-1,2}, {110}, {1-13}, {112}, and {2-21} were used for the simulations.

Diffraction patterns from the twin and parent match the simulations well, as shown in Fig. 9. Furthermore, comparison of the slip plane traces with potential slip systems – <a> basal, <a> prismatic, and <c + a> pyramidal – confirm that these slip traces are <a> prismatic which is the slip system with the lowest critical resolved shear stress in this material [21].

This example demonstrates that lower symmetry materials can be correctly represented. This is best highlighted through accurate reproduction of the diffraction patterns. Furthermore, it also highlights that analysis of slip bands from unknown slip systems can act as an indirect (but not conclusive) check for consistency between the sample map and the underlying crystal orientation. This case is not conclusive as it does not verify the 180° rotation between sample map and crystal orientations, as surface trace analysis is insensitive to this 180° rotation.

4. Discussion

This paper has outlined a method to accurately capture conventions used to describe crystal orientations with EBSD. Conventions used by different manufacturers, and potentially instruments, may be different and this generates complications when importing the data into 3rd party software for further analysis. We note that the definition of the sample reference frame underpins any description of rotation between reference crystal orientation and test orientation, and therefore this frame must be described with extreme care and clarity. This is in addition to a precise description of the reference unit cell within this frame and the relationship between map grid, sample geometry, and detector position.

The examples presented here and fundamental assessment of beam shift and EBSP coordinate systems can be used to confidently establish a consistent convention for use by any EBSD users.

At a minimum, analysis of a single crystal of silicon will inform the user of the orientation of the EBSP image with respect to the mapped coordinate system. As much EBSD analyses focusses only on the surface plane of a sample, a rotation of 180° about the surface normal may be missed. To check this issue requires careful analysis of a particular microstructural feature in 3D, such as the habit plane of a coherent {111} twin plane in Ni, in 3D which requires precise knowledge of the out of plane crystal direction.

Lower symmetry materials can represent further complications with EBSD analysis. Significant development of EBSD systems focussed almost exclusively on highly symmetric cubic materials, and so simple conventions involving the alignment of the reference crystal with particular external reference frames is often overlooked. This can be found when comparing data from one system with another and, for example in HCP materials, the direction of the <a> axis is either parallel to the X or Y axis in the reference configuration that can render a 30° rotation error with respect to

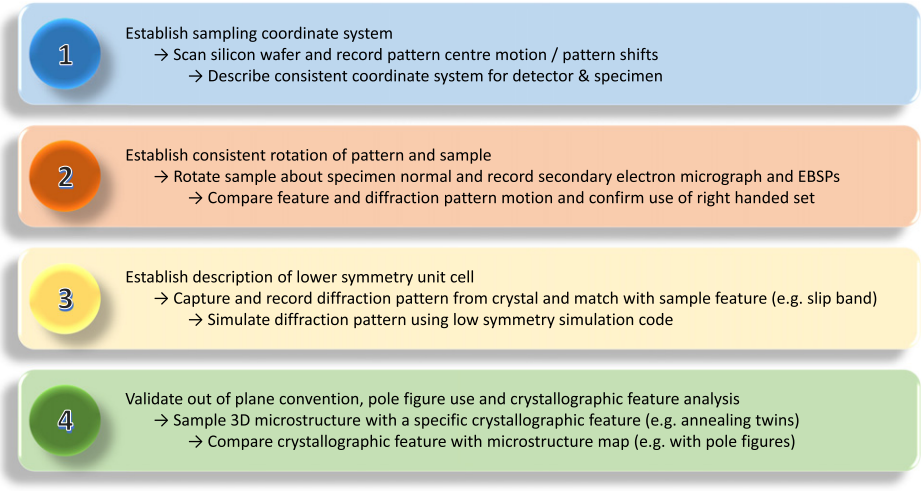

Fig. 10. Recommendations to validate a consistent description of scanning coordinates and description of a crystallographic unit cell as described in the sample coordinate system.

interpretation of the crystal orientation perpendicular to the <c> axis. In many EBSD analyses, especially of cubic systems, this is unimportant. However increasing application of EBSD to study lower symmetry materials, such as titanium and many common geological minerals, requires more precise descriptions of the reference cell.

In many instances use of EBSD data is confined to direct analysis within the highly sophisticated software tools provided by the manufacturers and many users will be content with these walled gardens. This is a strong statement of support for the excellent work by each of the manufacturers to take a complicated technique and make it tractable to solve real engineering challenges. However, for many intermediate and advanced users data is routinely taken out of these gardens and explored in 3rd party tools, such as MATLAB® using MTEX [22–24], crystal plasticity tools [25,26], further computational processing such as HR-EBSD [27–29], or sophisticated packages for microstructural analysis such as Dream3D [30]. Here precise knowledge of conventions employed as well as use of simple unambiguous validation samples will provide increased confidence in results obtained from supplied hardware and software systems.

In practice not all of the examples shown here are required to validate the use of crystal orientation, but each in turn offers a subtle change in complexity that can be used to diagnose where a chosen convention is not behaving as expected. Formally, representation of a low symmetry example combined with the sub-surface sectioning would be sufficient, however it is unlikely that most labs have routine access to a sample of this sort.

Users are recommended to perform a beam scan on a silicon single crystal wafer that establishes whether the beamshift and pattern representation are behaving as expected. The handedness of the axis systems in the sample and EBSP can be validated with a simple rotation of the sample about the surface normal (a change in tilt is possible but complex if the sample is not mounted in a eucentric position). Then sectioning of a cubic sample containing coherent twins can verify the out of plane orientation and reproduction of an EBSP from a lower symmetry crystal, such as the titanium example shown here, would confirm that the unit cell in the reference orientation is reasonable. A summary of our recommended approach is outlined in Fig. 10.

5. Recommendations

EBSD is a commonly used technique that fundamentally interprets a diffraction pattern to understand the unit cell many times to generate rich microstructure maps. In light of increasing access to data, as well as new and exciting data analysis strategies, it is important that both users and manufacturers offer suitable descriptors of their data.

We suggest the following:

Users test their conventions using one or more of the strategies outlined above.

Testing accurate reproduction of a suitable convention should be part of the acceptance trial of any new EBSD system.

Manufacturers store data with sufficient information that reproduction of examples above are routine and transparent. This may include provision of exemplar code in a simple language (we suggest Python as this is a free and simple to read language).

Data is stored in a more accessible format with plain language meta data and that suitable methods to store patterns, coordinate maps, and interpreted crystallographic data are easily readable with common data formats (we are excited by coordinated efforts which suggest integrated formats, such as the HDF5 data format proposed by Jackson et al. [16,31]).

6. Conclusions

EBSD is a routinely used crystallographic measurement tool and advanced software packages supplied with hardware systems can be used for sophisticated analysis of microstructural components. Care must be taken when considering numerous conventions required to describe: (a) the crystallographic unit cell in a reference configuration; (b) the relationship of this reference configuration to the recorded diffraction pattern; (c) the relationship between the recorded diffraction pattern and the scanned microstructural map. If the user wants to extend beyond these tools and export the data for third party analysis, or validate their analysis with the software packages, then a series of experiments outlined here can be performed to confidently (and independently) verify the convention used to describe crystal orientation.

Acknowledgements

The authors would like to thank Thomas Schwager (Bruker Nano GmbH) for helpful discussions and the suggested convention for describing a unit cell.

The authors would like to thank a range of funders that underpin this collaborative work: T.B. Britton has a fellowship from the Royal Academy of Engineering. J. Jiang is funded by AVIC BIAM. T.B. Britton and A.J. Wilkinson have project funding from EPSRC through the HexMat programme grant (www.imperial.ac.uk/hexmat EP/K034332/1). DW, A. J. Wilkinson and L. Henson have project funding from NERC through NE/M000966/1. A.J. Wilkinson and A. Vilalta-Clemente have project funding from EPSRC through EP/J016098/1.

Appendix A

Use of the crystal orientation shown in Example 3.
The pattern was indexed with:
Pattern centre: [$PC_x = 0.48$, $PC_y = 0.28$, $DD = 0.64$]
Euler angles: [$\phi_1 = 127°, \Phi = 38°, \phi_2 = 273°$]
Detector tilt = 5°
Sample tilt = 70°.
This results in the following rotation matrices:

$$\boldsymbol{R}_{z(\phi_1)} = \begin{pmatrix} -0.6018 & 0.7986 & 0 \\ -0.7986 & 0.6018 & 0 \\ 0 & 0 & 1 \end{pmatrix}$$

$$\boldsymbol{R}_{x(\Phi)} = \begin{pmatrix} 1 & 0 & 0 \\ 0 & 0.7880 & 0.6157 \\ 0 & -0.6157 & 0.7880 \end{pmatrix}$$

$$\boldsymbol{R}_{z(\phi_2)} = \begin{pmatrix} 0.0523 & -0.9986 & 0 \\ 0.9986 & 0.0523 & 0 \\ 0 & 0 & 1 \end{pmatrix}$$

$$\boldsymbol{R}_{x(\alpha)} = \begin{pmatrix} 1 & 0 & 0 \\ 0 & 0.9063 & -0.4226 \\ 0 & 0.4226 & 0.9063 \end{pmatrix}.$$

Which can be combined to generate:

$$\boldsymbol{G}_{sample} = \begin{pmatrix} 0.5970 & 0.5154 & -0.6148 \\ -0.6339 & 0.7727 & 0.0322 \\ 0.4917 & 0.3705 & 0.7880 \end{pmatrix}$$

phi1,Phi,phi2:

(2.2113321622768156, 0.6614797865058508, 4.750786223928564)

(126.7, 37.899999999999999, 272.19999999999999)

U_S = Rx(alpha):

[[1. 0. 0.]

 [0. 0.90938136 -0.41596338]

 [0. 0.41596338 0.90938136]]

Rz(phi1):

[[-0.59762515 0.80177564 0.]

 [-0.80177564 -0.59762515 0.]

 [0. 0. 1.]]

Rx(Phi):

[[1. 0. 0.]

 [0. 0.78908408 0.6142852]

 [0. -0.6142852 0.78908408]]

Rz(phi2):

[[0.03838781 -0.99926292 0.]

 [0.99926292 0.03838781 0.]

 [0. 0. 1.]]

U_O = G_sample:

[[0.60926055 0.50200731 -0.61383242]

 [-0.6214714 0.78308188 0.02358106]

 [0.49251891 0.36711228 0.78908408]]

U_O*U_S = G_detector:

[[0.60926055 0.20118428 -0.76702442]

 [-0.6214714 0.72192893 -0.30428921]

 [0.49251891 0.66207515 0.56487309]]

U_K=U_A*U_O*U_S:

[[0.60926055 0.20118428 -0.76702442]

 [-0.6214714 0.72192893 -0.30428921]

 [0.49251891 0.66207515 0.56487309]]

Structure Matrix A:

[[1.00000000e+00 0.00000000e+00 0.00000000e+00]

 [6.12323400e-17 1.00000000e+00 0.00000000e+00]

 [6.12323400e-17 6.12323400e-17 1.00000000e+00]]

column vector, direct lattice:

[[1]

[2]

[-3]]

column vector, sample frame:

[[-2.11123899]

[0.96683422]

[-2.93392255]]

column vector, detector frame:

[[-2.11123899]

[-0.34118333]

[-3.07022212]]

$$\boldsymbol{G}_{detector} = \begin{pmatrix} 0.5970 & 0.2073 & -0.7750 \\ -0.6339 & 0.7139 & -0.2974 \\ 0.4917 & 0.6688 & 0.5576 \end{pmatrix}.$$

This can be used to rotate an example vector:

$$\mathbf{v_K} = [1 \quad 2 \quad -3]$$

$$\mathbf{v_{detector}} = \mathbf{v_K G}_{\text{detector}} = [-2.15 \quad -0.37 \quad -3.04]$$

$$\mathbf{v_{sample}} = \mathbf{v_K G}_{\text{sample}} = [-2.15 \quad 0.95 \quad -2.91].$$

Python plotEBSDLatticeGeo.py for Ni_Example3.bmp:

Appendix B. Supplementary data

Supplementary data to this article can be found online at http://dx.doi.org/10.1016/j.matchar.2016.04.008.

References

[1] B.L. Adams, S.I. Wright, K. Kunze, Orientation imaging: the emergence of a new microscopy, Metallurgical Transactions A 24A (1992) 819–831.
[2] N.C. Krieger Lassen, D. Juul Jensen, K. Conradsen, Image-processing procedures for analysis of electron back scattering patterns, Scanning Microsc. 6 (1992) 115–121.
[3] N.C. Krieger Lassen, D. Juul Jensen, K. Conradsen, Automatic recognition of deformed and recrystallized regions of partly recrystallized samples using electron back scattering patterns, Mater. Sci. Forum 157-162 (1994) 149–158.
[4] A.J. Wilkinson, T.B. Britton, Strains, planes, and EBSD in materials science, Mater Today 15 (2012) 366–376.
[5] D. Dingley, Progressive steps in the development of electron backscatter diffraction and orientation imaging microscopy, J. Microsc. (Oxford) 213 (2004) 214–224.
[6] F.J. Humphreys, Review - grain and subgrain characterisation by electron backscatter diffraction, J. Mater. Sci. 36 (2001) 3833–3854.
[7] D. Viladot, M. Veron, M. Gemmi, F. Peiro, J. Portillo, S. Estrade, J. Mendoza, N. Llorca-Isern, S. Nicolopoulos, Orientation and phase mapping in the transmission electron microscope using precession-assisted diffraction spot recognition: state-of-the-art results, J. Microsc. 252 (2013) 23–34.
[8] I. Ghamarian, Y. Liu, P. Samimi, P.C. Collins, Development and application of a novel precession electron diffraction technique to quantify and map deformation structures in highly deformed materials-as applied to ultrafine-grained titanium, Acta Mater. 79 (2014) 203–215.
[9] A.C. Leff, C.R. Weinberger, M.L. Taheri, Estimation of dislocation density from precession electron diffraction data using the Nye tensor, Ultramicroscopy 153 (2015) 9–21.
[10] R.R. Keller, R.H. Geiss, Transmission EBSD from 10 nm domains in a scanning electron microscope, J. Microsc. 245 (2012) 245–251.
[11] S. Suzuki, Evaluation of transmission-EBSD method and its application to observation of microstructures of metals, J. Jpn. I Met. 77 (2013) 268–275.
[12] Y. Guo, D.M. Collins, E. Tarleton, F. Hofmann, J.Z. Tischler, W. Liu, R. Xu, A.J. Wilkinson, T.B. Britton, Measurements of stress fields near a grain boundary: exploring block arrays of dislocations in 3D, Acta Mater. (2015).
[13] F.P.E. Dunne, Fatigue crack nucleation: mechanistic modelling across the length scales, Curr. Opin. Solid St. M. 18 (2014) 170–179.
[14] P. Eisenlohr, M. Diehl, R.A. Lebensohn, F. Roters, A spectral method solution to crystal elasto-viscoplasticity at finite strains, Int. J. Plast. 46 (2013) 37–53.
[15] D.J. Rowenhorst, A.D. Rollett, G.S. Roher, M.A. Groeber, M.A. Jackson, P.J. Konijnenberg, M. De Graef, Tutorial: consistent representations of and conversions between 3D rotations, Model. Simul. Mater. Sci. Eng. 23 (2015) 083501.
[16] M.A. Jackson, M.A. Groeber, M.D. Uchic, D.J. Rowenhorst, M. De Graef, h5ebsd: an archival data format for electron back-scatter diffraction data sets, Integrating Materials and Manufacturing Innovation 3 (2014).
[17] D. McKie, C. McKie, Essentials of Crystallography, Blackwell Scientific Publications, 1986.
[18] R.W. Fonda, K.E. Knipling, D.J. Rowenhorst, EBSD analysis of friction stir weld textures, Jom-Us 66 (2014) 149–155.
[19] U. Müller, Symmetry Relationships between Crystal Structures, Oxford University Press, 2013.
[20] H.-J. Bunge, Texture Analysis in Materials Science Butterworths, 1982.
[21] J.C. Gong, A.J. Wilkinson, Anisotropy in the plastic flow properties of single-crystal alpha titanium determined from micro-cantilever beams, Acta Mater. 57 (2009) 5693–5705.
[22] F. Bachmann, R. Hielscher, H. Schaeben, Grain detection from 2d and 3d EBSD data-specification of the MTEX algorithm, Ultramicroscopy 111 (2011) 1720–1733.
[23] R. Hielscher, H. Schaeben, A novel pole figure inversion method: specification of the MTEX algorithm, J. Appl. Crystallogr. 41 (2008) 1024–1037.
[24] V.A. Yardley, S. Fahimi, E.J. Payton, Classification of creep crack and cavitation sites in tempered martensite ferritic steel microstructures using MTEX toolbox for EBSD, Mater Sci Tech-Lond 31 (2015) 547–553.
[25] T.T. Zhang, D.M. Collins, F.P.E. Dunne, B.A. Shollock, Crystal plasticity and high-resolution electron backscatter diffraction analysis of full-field polycrystal Ni superalloy strains and rotations under thermal loading, Acta Mater. 80 (2014) 25–38.
[26] T.B. Britton, H. Liang, F.P.E. Dunne, A.J. Wilkinson, The effect of crystal orientation on the indentation response of commercially pure titanium: experiments and simulations, P R Soc A 466 (2010) 695–719.
[27] T.B. Britton, J. Jiang, P.S. Karamched, A.J. Wilkinson, Probing deformation and revealing microstructural mechanisms with cross-correlation-based, high-resolution electron backscatter diffraction, Jom-Us 65 (2013) 1245–1253.
[28] A.J. Wilkinson, E.E. Clarke, T.B. Britton, P. Littlewood, P.S. Karamched, High-resolution electron backscatter diffraction: an emerging tool for studying local deformation, J. Strain Anal. Eng. 45 (2010) 365–376.
[29] A.J. Wilkinson, G. Meaden, D.J. Dingley, High-resolution elastic strain measurement from electron backscatter diffraction patterns: new levels of sensitivity, Ultramicroscopy 106 (2006) 307–313.
[30] I.M. Robertson, C.A. Schuh, J.S. Vetrano, N.D. Browning, D.P. Field, D.J. Jensen, M.K. Miller, I. Baker, D.C. Dunand, R. Dunin-Borkowski, B. Kabius, T. Kelly, S. Lozano-Perez, A. Misra, G.S. Rohrer, A.D. Rollett, M.L. Taheri, G.B. Thompson, M. Uchic, X.L. Wang, G. Was, Towards an integrated materials characterization toolbox, J. Mater. Res. 26 (2011) 1341–1383.
[31] M. Jackson, J.P. Simmons, M. De Graef, MXA: a customizable HDF5-based data format for multi-dimensional data sets, Model Simul Mater Sc 18 (2010).